International Conference on Control, Engineering & Information Technology (CEIT'14)
Proceedings - Copyright IPCO-2014, pp.196-202
ISSN 2356-5608

Sensorless Vector Control of Induction Motor Supply by photovoltaic Generator

Hamza Bouzeria
Department of Electrical Engineering
University Hadj Lakhdar
Batna 05000, Algeria
bhamza23000@gmail.com

Cherif Fetha
Department of Electrical Engineering
University Hadj Lakhdar
Batna 05000, Algeria
cheriffetha@gmail.com

Tahar Bahi
Department of Electrical Engineering
University Badji Mokhtar
Box 12, 23000 Annaba, Algeria
tbahi@hotmail.com

Lotfi Rachedi
Department of Electrical Engineering
University Hadj Lakhdar
Batna 05000, Algeria
nouflout@yahoo.fr

Salima Lekhchine
Department of Electrical Engineering
University Badji Mokhtar
Box 12, 23000 Annaba, Algeria
slekhchine@yahoo.fr

***Abstract* - This paper presents an implementation of intelligent speed controller for induction motor drive. The classic PI and fuzzy logic controllers are used in vector control scheme indirect, where induction motor is fed by photovoltaic generator. Thus, the proposed structure in our work consists of a photovoltaic generator associated with the DC / DC converter controlled by the technique of fuzzy logic to provide maximum power. Moreover, adaptation of the rotor time constant powered by a photovoltaic solar energy, the latter control system adopts inverter current control scheme with variable hysteresis band. The simulation results Matlab / Simulink show that the controller performance in both transient and steady state is more satisfactory.**

Index Terms - photovoltaic; fuzzy logic controller; induction motor;MPPT.

I. INTRODUCTION

The increasing of the world energy of the demand for electricity has grown steadily in recent years has forced the research to the design and development of renewable energy sources such as the photovoltaic (PV). Nowadays photovoltaic energy is one of the most popular sources since it is clean, inexhaustible and requires little maintenance [1]. The PV power conversion has been an active research topic for renewable energy conversion applications [2]. However, Algeria has remotely isolated rural areas posed problems to rural energy management and development of renewable energy sources. The average annual daily solar radiation on a horizontal plane, it is within the range of 5–7 kWh/m²/day [3]. The PVis non-linear, so its optimum operating point depends on the temperature, the irradiation and the load variations. This point is called the Maximum Power Point (MPP), so the maximum power point tracking (MPPT) is usually used as online control strategy of chopper for to track the maximum output power operating point of the photovoltaic generator (PVG) for different operating climatic conditions. The continues voltage of DC-DC converter is obtained by MPPT algorithm based of fuzzy logic [4].There are different types of MPPT algorithms like for example perturbation and observation (P&O) method, incremental conductance method, which can be known as traditional techniques [5,6]. So, there are other techniques called artificial intelligence are becoming useful as alternate approach for conventional modeling techniques as they do not require the knowledge of internal system parameters, involve less computational effort and offer a compact solution for multivariable problems. They have been used to solve complicated practical problems in various areas and are becoming more popular in PV systems that exhibits non-linear features. There are two artificial intelligence techniques types: artificial neural networks (ANN) and fuzzy logic (FL) that used to design the MPPT controller for PV system [7].Currently at this time, the induction motor (IM) is by far the most used in industrial applications where variable speed with high precision control and high torque performance are required. Because it is robust, simple, cost-effective and least expensive [8]. Alternatively, the development of algorithms direct torque control or also known as vector control by the flow direction, Both direct and indirect field oriented control(IFOC)is essentially different in the angle calculation of Park θs (core size in the order) representing the phase of the faces in the reference related to the stator flux: in the indirect control this angle is calculated from the stator angular ωs, itself reconstituted using the autopilot which adds the electrical relationship ω speed and slip pulse ωg, while the direct control, directly calculates this angle from the measured or estimated values [9].The objective of this paper is to compare the performance of IFOC using two types of current regulators: the PI and FL improve the control strategy.

II. DESCRIPTION OF SYSTEM

The indirect field oriented control scheme considered in this work is given in Fig. 1. The drive consists PVG, converters, and IM.

International Conference on Control, Engineering & Information Technology (CEIT'14)
Proceedings - Copyright IPCO-2014, pp.196-202
ISSN 2356-5608

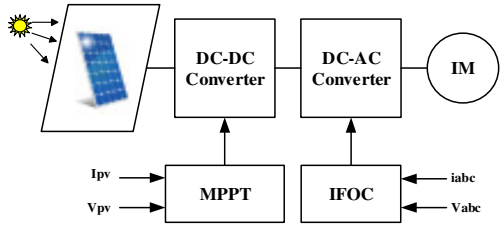

Fig. 1 Scheme of photovoltaic system.

A. *Modeling of Photovoltaic array*

The direct conversion of the solar energy into electrical power is obtained by solar cells. Solar cells as they are often called are semiconductor devices that convert sunlight into direct current electricity. Groups of PV cells are electrically configured into modules and arrays. The solar cell may be modeled by a current source in parallel with a diode, so shunt and a series resistance are added to the model. The equivalent circuit of solar cell is shown in Fig. 2.

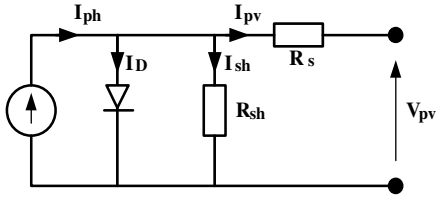

Fig. 2 Equivalent circuit for a solar cell.

The PV panel is composed of NP parallel modules. Each one including NS photovoltaic cell serial connected. The fundamental equation for PV model is given by (1) [10]:

$$I_{pv} = N_p\, I_{ph} - N_p I_0 \left\{\exp\left[\frac{q(V_{pv}+I_{pv}R_s)}{akTN_s}\right] - 1\right\} - \frac{V_{pv}+I_{pv}R_S}{R_{sh}} \quad (1)$$

$$I_0 = I_{or}\left(\frac{T}{T_r}\right)^3 \exp\left\{\frac{qE_G}{ka}\left[\frac{1}{T_r} - \frac{1}{T}\right]\right\} \quad (2)$$

$$I_{ph} = \{I_{sc} + k_i(T - 298)\}\frac{G}{1000} \quad (3)$$

where,

I_{pv}	: PV panel output current
V_{pv}	: V panel output voltage
I_{ph}	: generated photocurrent
R_{sh}, R_s	: parallel and series resistance, respectively
q	: electron charge
k	: Boltzmann's constant
a	: p–n junction ideality factor
I_0, I_{0r}	: real and reference cell reverse saturation current, respectively
k_i	: temperature coefficient for short circuit current
T, T_r	: real and reference temperature, respectively
I_{sc}	: short-circuit current
G	: solar radiation

B. *Modeling of converters*

Due to the change of temperature and solar irradiation, the PV module provides power to the load via a regulated converter to maintain maximum power. The chopper amplifier circuit considered is shown in Fig. 3.

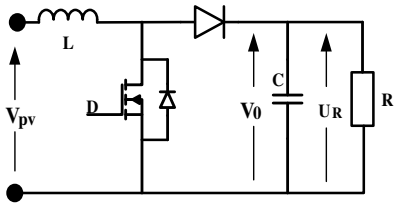

Fig. 3 DC-DC Converter Circuit.

In steady state, the output voltage of the chopper amplifier can be expressed by the following equations [11]:

$$V_0 = \frac{V_{pv}}{1-D} \quad (4)$$

$$V_0 = U_R \quad (5)$$

Concerning the modeling of the inverter whose circuit diagram is seen in Fig. 4. Considering the chopper control, the voltage V0is applied to the inverter input terminals of two capacitors (C1 and C2) used to create the midpoint fictitious.

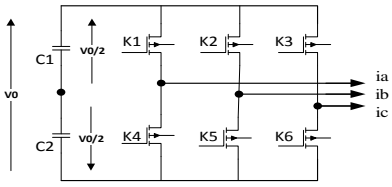

Fig. 4 Circuit of the three-phase inverter.

Tension arm at the midpoint of the DC link is expressed by the following equations [12]:

$$\begin{cases} V_{io} = +\frac{V_0}{2} \text{ if } \quad K_i = 1 \text{ avec } (i = 1,2,3) \\ V_{io} = -\frac{V_0}{2} \text{ if } \quad K_i = 1 \text{ avec } (i = 4,5,6) \end{cases} \quad (6)$$

And, the phase voltages at the terminals of the load are:

$$\begin{cases} U_{An} = \frac{2}{3}U_{A0} - \frac{1}{3}U_{B0} - \frac{1}{3}U_{C0} \\ U_{Bn} = -\frac{1}{3}U_{A0} + \frac{2}{3}U_{B0} - \frac{1}{3}U_{C0} \\ U_{Cn} = -\frac{1}{3}U_{A0} - \frac{1}{3}U_{B0} + \frac{2}{3}U_{C0} \end{cases} \quad (7)$$

With,

$$U_n = \frac{1}{3}(U_{A0} + U_{B0} + U_{C0}) \quad (8)$$

C. *Modeling of induction*

The dynamic model of the induction motor in the synchronous reference may be in the form of the following state equation [13]:

$$\begin{cases} \frac{di_{ds}}{dt} = \frac{1}{\sigma L_s}\left[-R_{sr}i_{ds} + \omega_s \sigma L_s i_{qs} + \frac{MR_r}{L_r^2}\Phi_{dr} + \frac{M}{L_r}\omega_r \Phi_{qr} + v_{ds}\right] \\ \frac{di_{qs}}{dt} = \frac{1}{\sigma L_s}\left[-R_{sr}i_{qs} - \omega_s \sigma L_s i_{ds} + \frac{MR_r}{L_r^2}\Phi_{qr} + \frac{M}{L_r}\omega_r \Phi_{dr} + v_{qs}\right] \\ \frac{d\Phi_{dr}}{dt} = \frac{MR_r}{L_s}i_{ds} - \frac{R_r}{L_r}\Phi_{dr} + \omega_g \Phi_{qr} \\ \frac{d\Phi_{qr}}{dt} = \frac{MR_r}{L_s}i_{qs} - \frac{R_r}{L_r}\Phi_{qr} + \omega_g \Phi_{dr} \end{cases} \quad (9)$$

$$T_e = n_p \frac{M}{L_r}\left(\Phi_{dr} i_{qs} - \Phi_{qr} i_{ds}\right) \quad (10)$$

$$J\frac{d\omega_r}{dt} + f\omega_r = T_e - T_L \quad (11)$$

where, $\omega_g = \omega_s - \omega_r$, $R_{sr} = \left(R_s + R_r \frac{M^2}{L_r^2}\right)$ and $\sigma = \left(1 - \frac{M^2}{L_s L_r}\right)$

Φ is the flux linkage; L: is the inductance; v: is the voltage; R:is the resistance; i: is the current; σ: is the motor leakage coefficient. ω_r is the rotor electrical speed. The subscripts r and s are the rotor and stator values respectively refereed to the stator, and the subscripts d and q denote the d-q axis components in the stationary reference frame. However, in the case of a supply voltage v_{ds} and v_{qs} influence on both i_{ds} and i_{qs}, so the flux and torque, which is the value of adding compensation terms to make d and q axes are completely independent. The performance brings the additional decoupling also told by compensation were shown in [14].

III. Indirect Field Oriented Control

The diagram block of IFOC for IM is shown in Fig. 5. It consists of two feedback control loops. The inner loop is a conventional synchronous current regulation loop. The torque command current, i_{qs}^*, is produced by selected controller in the outer speed loop, based on the command speed ω_r^* and the actual speed ω_r[15,16].The success of FOC is based on the proper division of stator current into two components: the torque component i_{qs}^* and magnetizing flux component i_{ds}^*. The indirect FOC method uses a slip equation for partitioning the stator current.

$$\omega_r^* = \frac{R_r i_{qs}^{e*}}{L_r i_{ds}^{e*}} \quad (12)$$

The axis are fixed on the stator, but the d_r-q_r axes, which are fixed on the rotor , are d_s-q_s moving at speed ω_r synchronously rotating axes d_e-q_e are rotating ahead of the d_r-q_r axes by the positive slip angle θ_s corresponding to slip frequency ω_{sl}. Since the rotor pole is directed on the de axes and $\omega_e=\omega_r+\omega_{sl}$ one can write:

$$\theta_e = \int \omega_e dt = \int (\omega_r + \omega_{sl})dt = \theta_r + \theta_{sl} \quad (13)$$

The phases diagram suggests that for decoupling control, the stator flux component of current i_{ds_e} should be aligned on the d_e axis and the torque component of current i_{qs_e} should be θ the q_e axis, as shown. For decoupling control, one can make a derivation of control equations of IFOC with the help of d_e-q_e dynamic model of IM. One can easily show the following important equations:

$$T_e = \frac{3PL_m}{4L_r}\left(\Phi_{dr}^e i_{qs}^e\right) \quad (14)$$

$$\Phi_{dr}^e = \frac{R_s L_m}{R_r + L_r P} i_{ds}^e \quad (15)$$

$$\omega_{sl}^e = \omega_s - \omega_r = \frac{R_r i_{ds}^e}{L_r i_{ds}^e} \quad (16)$$

IV. Speed And Flux estimation

Many schemes based on simplified motor models have been devised to sense the speed of the induction motor from measured terminal quantities for control purposes. In order to obtain an accurate dynamic representation of the motor speed, it is necessary to base the calculation on the coupled circuit equations of the motor. However, the performance of these methods is deteriorated at a low speed because of the increment of nonlinear characteristic of the system. The current paper proposes a new rotor speed estimation method to improve the performance of a sensorless vector controller in the low speed region and at zero speed. From the stator voltage equations in the stationary frame it is obtained [17]:

$$\begin{cases} \frac{d\Phi_{dr}}{dt} = \frac{L_r}{L_m}\left(v_{ds} - R_s i_{ds} - \sigma L_s \frac{di_{ds}}{dt}\right) \\ \frac{d\Phi_{qr}}{dt} = \frac{L_r}{L_m}\left(v_{qs} - R_s i_{qs} - \sigma L_s \frac{di_{qs}}{dt}\right) \end{cases} \quad (17)$$

Using the rotor flux and motor speed, the stator current is represented as:

$$\begin{cases} i_{ds} = \frac{1}{L_m}\left(\Phi_{dr} + \omega_r T_r \Phi_{qr} - T_r \frac{d\Phi_{dr}}{dt}\right) \\ i_{qs} = \frac{1}{L_m}\left(\Phi_{qr} - \omega_r T_r \Phi_{dr} - T_r \frac{d\Phi_{qr}}{dt}\right) \end{cases} \quad (18)$$

where, $T_r=L_r/R_r$ is the rotor time constant.

From the equations (17) and (18) and using the estimated speed, the stator current is estimated as:

$$\begin{cases} i_{ds}^e = \frac{1}{L_m}\left(\Phi_{dr} + \omega_r^e T_r \Phi_{qr} - T_r \frac{d\Phi_{dr}}{dt}\right) \\ i_{qs}^e = \frac{1}{L_m}\left(\Phi_{qr} - \omega_r^e T_r \Phi_{dr} - T_r \frac{d\Phi_{qr}}{dt}\right) \end{cases} \quad (19)$$

Where, i_{ds}^e and i_{qs}^e are the estimated stator currents and ω_r^e is the estimated rotor electrical speed. The vector control rotor flux oriented is called direct or indirect method to estimate the rotor flux vector.

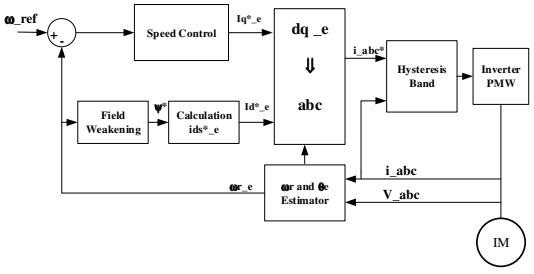

Fig. 5 Block diagram of IFOC scheme based IM drive.

International Conference on Control, Engineering & Information Technology (CEIT'14)
Proceedings - Copyright IPCO-2014, pp.196-202
ISSN 2356-5608

V. Adaptive Current Hysteresis Band Control

The hysteresis band is used to control load currents and determine switching signals for inverters gates. Suitable stability, fast response, high accuracy, simple operation, inherent current peak limitation and load parameters variation independency make the current control methods of voltage source inverters.

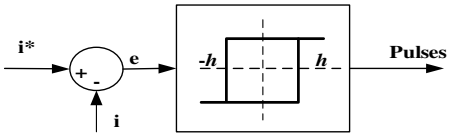

Fig. 6 Principle of Hysteresis Current Control.

In this approach the current error is difference between the reference current, and the current being injected by the inverter $e(t)= I_{ref}(t) - i_{Inj}(t)$. When the error current exceeds the upper limit of the hysteresis band, the upper switch of the inverter arm is turned OFF and the lower switch is turned ON. When the error current crosses the lower limit of the hysteresis band (HB), the lower switch of the inverter arm is turned OFF and the upper switch is turned ON [18]. As a result, the current gets back into the hysteresis band. The switching performance as follows:

$$s = \begin{cases} 0 & \text{if } i_{Inj}(t) > i_{ref}(t) + HB \\ 1 & \text{if } i_{Inj}(t) < i_{ref}(t) - HB \end{cases} \quad (20)$$

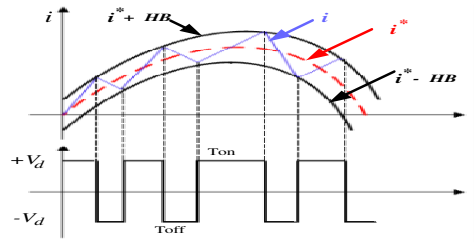

Fig. 7 Principle of Hysteresis Current Control.

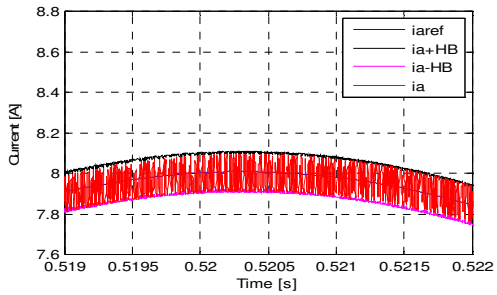

Fig. 8 Simulation of Hysteresis Current Control.

VI. Fuzzy Logic Controller

The maximum power that can be delivered by a PVG depends greatly on the insulation level and the operating temperature. Therefore, it is necessary to track the MPP all the time. They have the advantage to be robust and relatively simple to design as they do not require the knowledge of the exact model. They do require on the other hand the complete knowledge of the operation of the PV system show in Fig. 9.

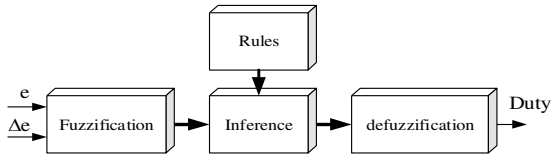

Fig. 9 General Diagram of Fuzzy Logic Controller.

The FLC input variables are the error (e) and derivate of error (Δe) at sampled times k defined by [19]:

$$\begin{cases} e(k) = \frac{P(k)-P(k-1)}{V(k)-V(k-1)} \\ \Delta e(k) = e(k) - e(k-1) \end{cases} \quad (21)$$

Where, P(k) is the instantaneous power of PVG. The FL tracks the MPP based on master rule of "*If X and Y, Then Z*" [20]. The fuzzy inference is carried out by using Mamdani's method and the defuzzification uses the center of gravity to compute the output of this FLC which is the optimum duty cycle The control rules are indicated in Table I with (e) and (Δe) as inputs and D as the output, where D is associated fuzzy sets involved in the fuzzy control rules .

TABLE I
Fuzzy Rules

Δe | e	NB	NM	NS	ZE	PS	PM	PB
NB	*NB*	*NB*	*NB*	*NB*	*NM*	*NS*	*ZE*
NM	*NB*	*NB*	*NB*	*NM*	*NS*	*ZE*	*PS*
NS	*NB*	*NB*	*NM*	*NS*	*ZE*	*PS*	*PM*
ZE	*NB*	*NM*	*NS*	*ZE*	*PS*	*PM*	*PB*
PS	*NM*	*NS*	*ZE*	*PS*	*PM*	*PB*	*PB*
PM	*NS*	*ZE*	*PS*	*PM*	*PB*	*PB*	*PB*
PB	*ZE*	*PS*	*PM*	*PB*	*PB*	*PB*	*PB*

VII. Simulation

Figure 10 shows the schema that is the basis of this study that fits in the field of renewable energy. The different parts are programmed to bases of their respective models and mainly two types of controllers are tested and their results analysed.

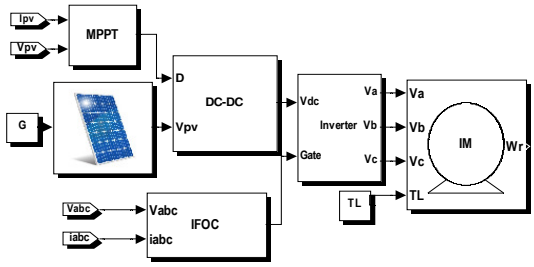

Fig. 10 Diagram Bloc Photovoltaic System.

International Conference on Control, Engineering & Information Technology (CEIT'14)
Proceedings - Copyright IPCO-2014, pp.196-202
ISSN 2356-5608

The results of simulations are presented in Fig. 11 and Fig. 12 respectively, for fuzzy control and the classic one. Each of them shows flow, the superposition of the set point and actual torque and the evolution of the real speed and estimates under different levels of precautions. Concerning Fig. 11, we note that the stream stabilizes at its value at the moment 0.35 s is will remain to this goes them whatever the variation of load torque. Furthermore, there is a good follow-up of the load torque and the two speeds (actual and estimated) are close.

In what is shown in Fig. 12, there is almost the same remarks as for the FLC command but the performance of the latter is better.

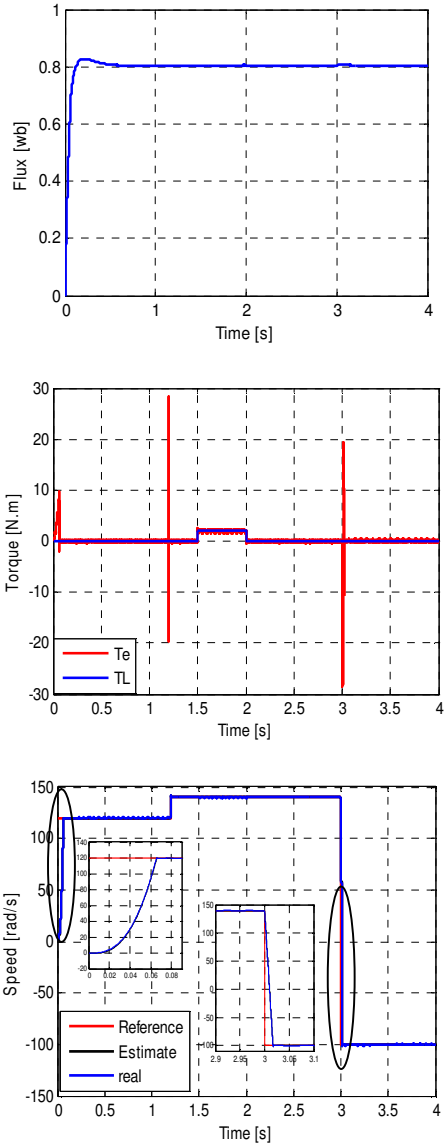

Fig. 11 Flux, torque and speed with FLC.

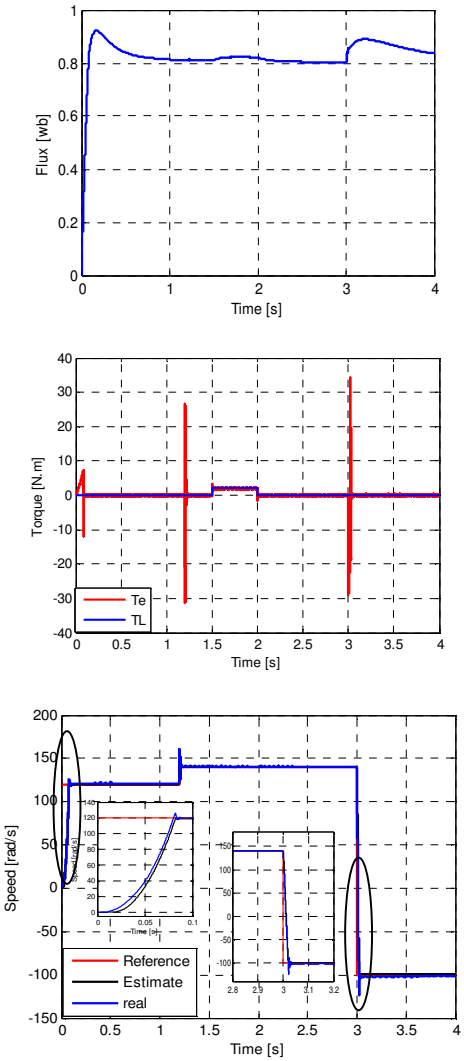

Fig. 12 Flux, torque and speed with PI.

VIII. Conclusion

This work has allowed analyzing the performance of the string photovoltaic for different regimes of operation and under different con-signs of speed especially. For the two cases analyzed the effectiveness of the uncoupling control and maintained even for a command without sensor. Also, the blur setting ensures best performance compared to the classical PI.

REFERENCES

[1] B. Prabodh, D. Vaishalee, "Hybrid renewable energy systems for power generation in standalone applications". *Renewable and Sustainable Energy Reviews*, vol 16 no. 5, pp. 2926-2939, june 2012.

[2] A. Chaouachi, M.K. Rashad, K. Nagasaka, "A novel multi-model neuro-fuzzy-based MPPT for three-phase grid-connected photovoltaic system". *Solar Energy*. vol. 84, no. 12, pp. 2219-2229, December 2010.

[3] L. Shuhui, A.H. Timothy, L. Dawen, H. Fei, "Integrating photovoltaic and power converter characteristics for energy extraction study of solar PV systems". *Renewable Energy.*vol. 36, no. 12, pp.3238-3245, 2011.

[4] Y. Himri, AS. Malik, A. BoudgheneStambouli, S. Himri, B. Draoui, "Review and use of the Algerian renewable energy for sustainable development". *Renewable and Sustain Energy Reviews*. vol. 36, pp. 1584-1591, 2009.

[5] R. Faranda, S. Leva, "Energy comparison of MPPT techniques for PV Systems". *WSEAS Transcations on Power Systems*, pp. 1-6,2008.

[6] A. Mellit, A.K. Soteris, "Artificial intelligence techniques for photovoltaic applications". *Elsevier -Progress in Energy and Combustion Science*. vol. 36, no. 5, pp. 574-632, October 2008.

[7] C. Ben Salah, M. Ouali, "Comparison of fuzzy logic and neural network in maximum power point tracker for PV systems". *Electric Power Systems Research*. Vol 81 n 1 pp 43-50 January(2011)

[8] M. Boussak, K. Jarray, "A High Performance Sensorless Indirect Stator Flux Orientation Control of Induction Motor Drive". *IEEE Transactions on Industrial Electronics*. vol. 53, no. 1, pp. 41-49, 2006.

[9] D. Fiaschi, al, "Improving the effectiveness of solar pumping systems by using modular centrifugal pumps with variable rotational speed". *SolarEnergy*. vol. 79, no. 3, pp. 234–244, September 2005.

[10] A. Kalirasu, S. SekarDash, "Simulation of Closed Loop Controlled Boost Converter for Solar Installation".*Serbian Journal of Electrical Engineering*.vol. 7, no. 1, pp, 121-130,2010.

[11] N. Mohan, T.M. Undeland, W.P. Robbins, "Power Electronics, Converters Applications and Design". John Wiley& Sons, Inc, 1995.

[12] A. Nasri, A. Hazzab, I. Bousserhane, S. Hadjeri, P. Si-card, "Two Wheel Speed Robust Sliding Mode Control for Electric Vehicle Drive". *Serbian Journal of Electrical Engineering*.vol. 5, no. 2, pp. 199-216 , 2008.

[13] M. Malinowski, " Sensorless Control Strategies for Three-Phase PWM Rectifiers", Ph.D. Thesis, Warsaw University of Technology, Warsaw, (2001)

[14] K. Bimal, K. Bose, "An Adaptive Hysteresis-Band Current Control Technique of a Voltage-Fed PWM Inverter for Machine Drive System". *IEEE Tran on Industrial Electronics.* Vol. 37, no. 5.pp. 402-408,1990.

[15] L. Malesani, P. Tenti, "A Novel Hysteresis Control Method for Current-Controlled Voltage-Source PWM Inverters with Constant Modulation Frequency". *IEEE Tran on Indu Elect,* vol. 26, no. 1, pp. 88-92, 1990.

[16] F.Z. Peng, T. Andfukao, "Robust Speed Identification for Speed Sensorless Vector Control of Induction Motors". *IEEE Trans.Indus. Applica*.vol. 30, no. 5, pp. 1234-1240, 1994.

[17] W. Parkc, H. Kwonw, "Simple and robust sensorless vector control of induction motor using stator current based MRAC".*Electric Power SystemsResearch*,vol. 71, no. 3, pp. 257-266, November 2004.

[18] R. Belaidi, A. Haddouche, H. Guendouz, "Fuzzy Logic Controller Based Three-Phase Shunt Active Power Filter for Compensating Harmonics and Reactive Power under Unbalanced Mains Voltages". *Energy Procedia*. vol. 18, pp. 560 – 570, 2012.

[19] N, Hamrouni, M. Jraid, A, Cherif, A, Dhouib, "Measurements and Simulation of a PV Pumping Systems Parameters Using MPPT and PWM ControlStrategies". *IEEE Melecon*.pp. 885- 888, 2006.

[20] S.G. Malla, C.N. Bhende, S. Mishra, "Photovoltaic based Water Pumping System", *International Conference Energy, Automation and Signal (ICEAS)*,pp .1-4, 2011.